Nuclear Inst. and Methods in Physics Research, A 1042 (2022) 167423

Contents lists available at ScienceDirect

Nuclear Inst. and Methods in Physics Research, A

journal homepage: www.elsevier.com/locate/nima

Resistive Micromegas high-rate and long-term ageing studies at the CERN Gamma Irradiation Facility

E. Farina [a,*], B. Alvarez Gonzalez [b], P. Iengo [a], L. Longo [c], J. Samarati [a], G. Sekhniaidze [d], O. Sidiropoulou [a], J. Wotschack [a,e]

[a] CERN, Esplanade des Particules 1, Meyrin, Switzerland
[b] Instituto Universitario de Ciencias y Tecnologías Espaciales de Asturias (ICTEA), Universidad de Oviedo, Oviedo, Spain
[c] INFN Lecce; Dipartimento di Matematica e Fisica, Università del Salento, Via per Arnesano, 73100, Lecce, Italy
[d] INFN Napoli, Strada Comunale Cintia, 80126 Naples, Italy
[e] Aristotle University of Thessaloniki, 540 06, Thessaloniki, Greece

ARTICLE INFO

Keywords:
Resistive micromegas
GIF++
Long-term ageing studies
High particle-rate performance

ABSTRACT

The LHC experiments are undergoing important upgrades for the High Luminosity LHC project. Experiments will be required to operate under three times higher instantaneous luminosity and higher levels of radiation when compared to LHC Run2. The integrated luminosity will increase by a factor ten. To cope with these conditions resistive Micromegas chambers were chosen by the ATLAS experiment as one of the technologies for the upgrade of the first forward muon stations. This paper describes the results of two prototype Micromegas detectors that were installed in the CERN Gamma Irradiation Facility with the aim to evaluate the detector performance under high-rate irradiation and to assess ageing effects over a 2.5 year long irradiation period and an accumulated charge in excess of 0.3 C/cm^2.

1. Introduction

Collider experiments will have to cope with higher and higher particle rates in the upcoming years. The capability of the detectors to work in such environments is thus a fundamental parameter to be taken into account in the choice of candidates for upgrades. A second important aspect to be considered is the ageing of the detectors under long-term exposure to ionizing radiation. In particular, the latter has been found to affect the performance of wire-based gaseous detectors, leading to a reduction of the amplification gain and a progressive degradation of the efficiency in particle detection [1]. This detrimental effect is the result of the deposition of material on either the anode or the cathode, in form of whiskers, droplets, or uniform coating.

This paper presents the characterization of two resistive bulk Micromegas detectors produced at CERN when operated with an Ar:CO_2 gas mixture and exposed to a high-rate background environment. It shows how their performance is affected over time in a long-term irradiation equivalent to about 10 years in the High Luminosity LHC (HL-LHC) environment, corresponding to an estimated accumulated charge of 0.2 C/cm^2 with a safety factor $\sim$ 2. The studies have been performed at the Gamma Irradiation Facility (GIF++) at CERN where a photon background from the radioactive decay of ^{137}Cs is combined with muons from the CERN SPS accelerator. The two detectors were the first Micromegas detectors ever that have been tested in GIF++.

This paper is organized as follows. Section 2 describes the facility where the studies are performed. In Section 3 the detector technology used for these studies is presented. Section 4 describes the data acquisition and clusterization algorithm, and Section 5 the simulation of the events. The results are presented in Section 6. Finally, in Section 7 the conclusions are drawn.

2. The CERN Gamma Irradiation facility

The Gamma Irradiation facility [2] at CERN is located in the SPS North Area, it is dedicated to studies in high particle-rate background and has been operational since March 2015. It combines a radioactive source, ^{137}Cs, having an initial activity of 13.9 TBq and a half-life of about 30 years, with muon and high-rate pion beams from the CERN SPS accelerator complex. The high source activity allows us to accumulate doses equivalent to HL-LHC experimental conditions in a reasonable amount of time. The source is equipped with lenses that equalize the photon flux on the x–y plane. The gamma rate reaching the detector can be modulated by a set of filters, partially shielding the source. The experimental setups are organized in two areas inside the bunker: the up-stream one, closer to the beam starting point, and the downstream one, on the source side where the beam leaves the bunker.

* Corresponding author.
E-mail address: edoardo.maria.farina@cern.ch (E. Farina).

https://doi.org/10.1016/j.nima.2022.167423
Received 13 February 2022; Received in revised form 11 July 2022; Accepted 31 August 2022
Available online 6 September 2022

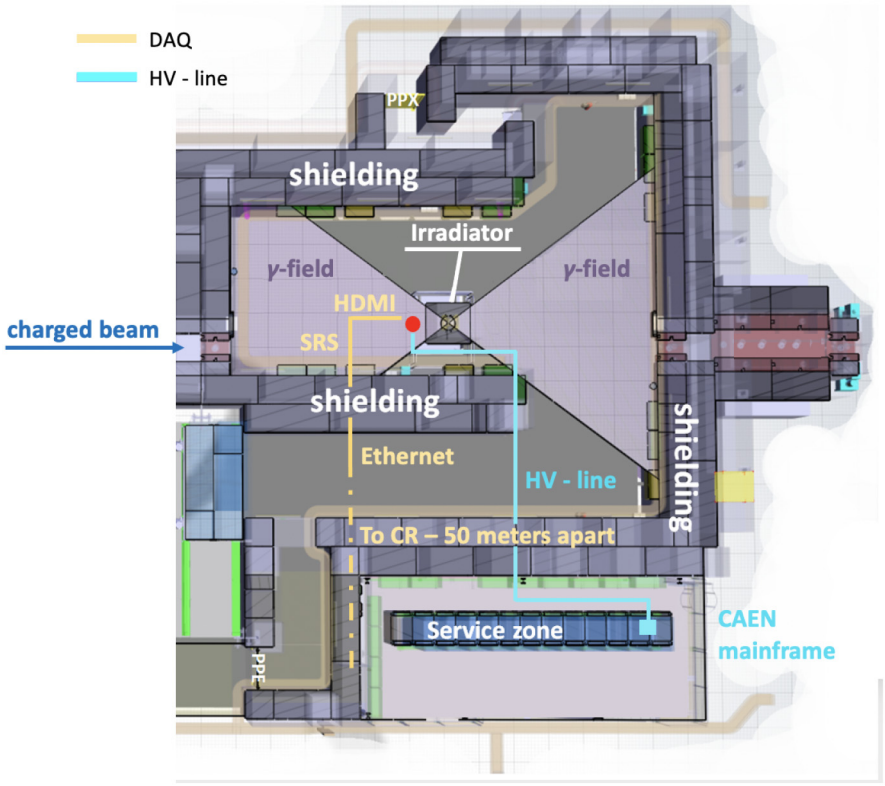

Fig. 1. Layout of the GIF++ facility during the data-taking period. The position where the Micromegas setup was installed is indicated by the red circle in the upstream area.

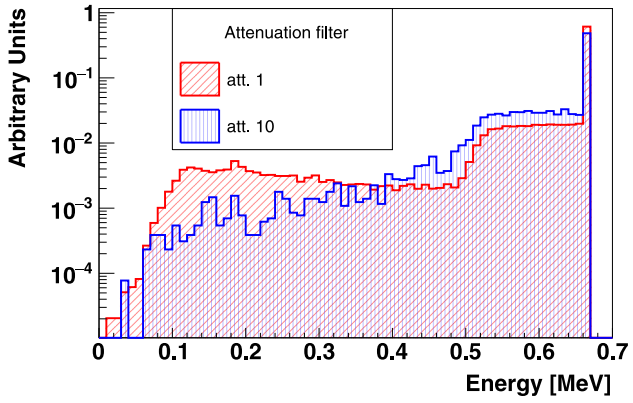

Fig. 2. Photon spectra as simulated at 1 metre from the source in the GIF++ facility. The distributions for attenuation filter 1 and 10 are normalized.

The attenuation filters are operated independently for these two areas. Attenuation filters act on top of the lenses.

The Micromegas detectors have been installed in the upstream area of the GIF++ facility on a vertical metallic stand facing the source at a distance of about 90 cm, as shown in Fig. 1. Fig. 2 shows the photon energy spectrum at 1 m from the source for filter settings 1 (i.e. source not shielded) and 10 (one tenth of the photon rate). About half of the photons have an energy of 662 keV, while the other half covers a wide range between 0 and 662 keV.

3. Micromegas detector

Micromegas [3] is a detector technology belonging to the category of parallel-plate Micro Pattern Gaseous Detectors (MPGDs). These detectors have been designed to overcome limitations of the wire-based gaseous detectors, mainly concerning the high-rate capability, the ageing and the resolution limited by the wire spacing. This technology is rapidly changing the paradigm of gaseous particle detectors, improving their limits. Many large experiments are foreseeing upgrade projects involving MPGD-based detectors.

The original Micromegas design consists of a drift electrode (cathode), a few-millimetre gas gap where the particles interact (called drift gap or gas gap), a metallic mesh and an anode layer where the signal is read out. The metallic mesh is kept at a well defined distance from the readout by insulating pillars (typical height 0.1 mm). The above-mentioned design was later improved by the resistive layer technology, consisting of an additional insulating layer dividing the anode and the readout pattern as shown in Fig. 3. This design has been found to reduce the impact of discharges on the detector [4].

The two Micromegas detectors that were used for these studies (called T5 and T8) were produced at CERN and profit of this resistive design. The detectors have an active area of 10×10 cm^2, with a 5 mm drift gap, and ≈100 μm amplification gap. The anode is made of screen-printed resistive strips on a 50 μm thick Kapton® layer. The readout plane is composed of 300 μm wide copper strips with a strip pitch of 400 μm. The mesh, separating the drift from the amplification gap, has 18 μm-thick wires, with an opening of 45 μm, it is embedded in the supporting pillars.

4. Data acquisition setup and clusterisation algorithm

The Micromegas detectors have been installed in the upstream area of the GIF++ facility at a distance of about 90 cm from the source. At this distance the photon rate has been estimated to be large enough to reach our desired accumulated charge of 0.2 C/cm^2, the equivalent integrated charge expected after 10 years of HL-LHC operation in the ATLAS Micromegas New Small Wheel (NSW) region [5], in about 2 years.

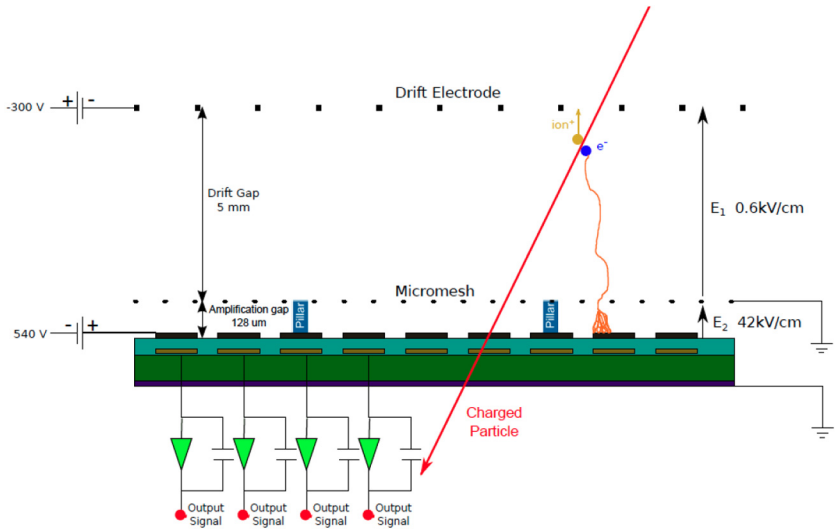

Fig. 3. Resistive Micromegas structure with a 5 mm drift gap, and ≈100 μm amplification gap.

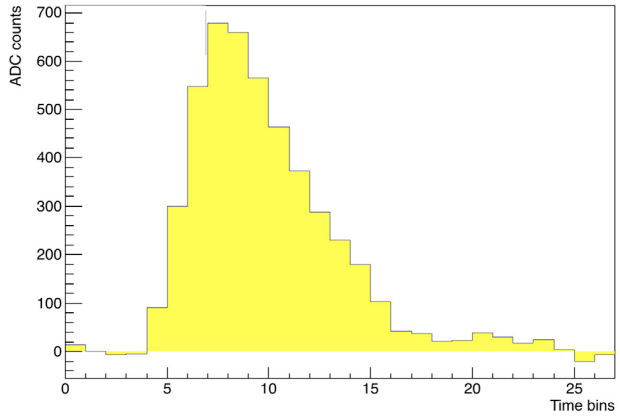

Fig. 4. Strip signal as acquired by the APV25 electronics.

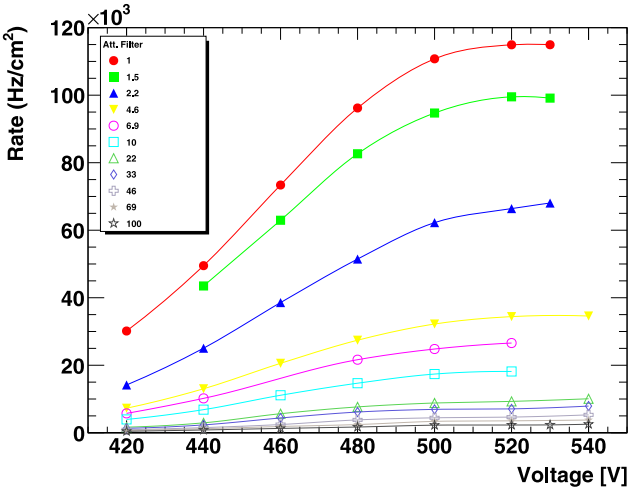

Fig. 5. Gamma conversion rate measured as a function of the amplification voltage for different values of source attenuation.

The detectors can slide horizontally on a rail with respect to the source position up to about 40 cm. This movement affects the rate of photons illuminating the detectors, resulting in a slightly different ageing rate between the two chambers. The impact of the detector

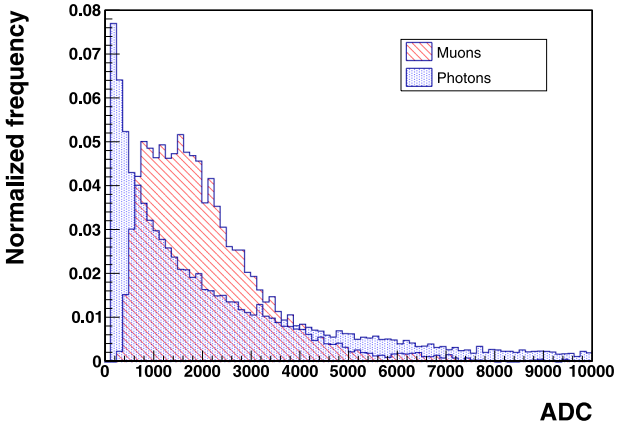

Fig. 6. Comparison between the cluster charge distributions (ADC counts) obtained when the detector is exposed to muons or photons.

positions with respect to the source has been studied by means of a Geant4 simulation [6], described in Section 5.

The detectors were operated with a 93:7 Ar:CO_2 gas mixture from a pre-mixed gas bottle, placed outside the facility, through copper and stainless steel pipes. The detector High Voltages (HVs), both amplification and drift, were remotely controllable — by means of a DCS (Detector Control System). The detector signals have been read by APV25 hybrids [7], directly mounted on the detectors, through the RD51 Scalable Readout System (SRS) [8]. The SRS Front-End and ADC cards were installed in the bunker close to the detector but shielded from radiation. From there the signals were routed through ethernet cables to the control room situated 50 m apart.

Ionizing particles depositing energy in the gas generate signals in one or more strips. A typical signal from a single readout strip, as acquired by the APV25 hybrid, is shown in Fig. 4. It shows the integrated charge, expressed in ADC counts,[1] for 27 time bins, each 25 ns wide. A fast signal rise, of the order of hundred nanoseconds, is followed by a slower decay. From each signal two parameters, in addition to the physical strip position, can be extracted: the maximum integrated charge and the time at which this maximum charge is reached.

Data coming from all strips belonging to the same ionizing event are then merged into so-called clusters. The cluster position and charge, the

[1] One ADC count corresponds approximately to 200 electrons.

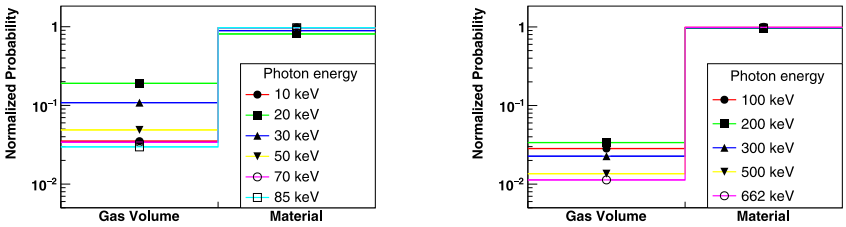

(a) (b)

Fig. 7. Normalized probability for depositing a detectable energy in the gas by a photon interaction in the gas (Gas Volume) and by photon interactions in the detector material (Material) for several energies of the primary photon.

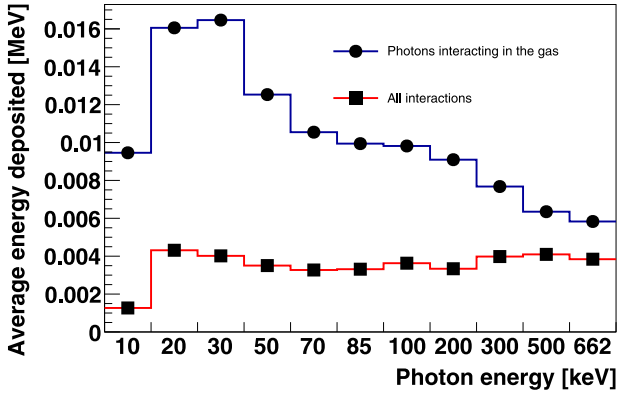

Fig. 8. Average energy deposited per event as a function of the energy of the simulated photon for events where the photon interacted in the gas (blue line) and for all photon interactions (red line).

arrival time, as well as total charge, size (in terms of strips fired), and the signal shape are retained. The cluster reconstruction that has been developed consists in merging adjacent strips (neighbouring strips), whose times of arrival are compatible with resulting from a single ionizing event. The cluster charge is then defined as the sum of the strip charges. In addition, to suppress noisy strips, strips with a charge smaller than 50 ADC counts are not considered in the clusterization. In order to account for inefficient channels, strips without signals can also be merged into the cluster if surrounded by two fired strips. Furthermore, a noise suppression algorithm is defined comparing the noise level in absence of signal (pedestal) with the actual signal.

At the highest photon rate, additional electronics noise has been observed resulting in a shift of the pedestal level, different event per event. To compensate this shift, a new baseline level is estimated from the first four and the last ten time bins of the signal shown in Fig. 4 and the strip signal is shifted by the difference between the pedestal and the new baseline. The cleaning algorithm has been tested against data taken in absence of noise to confirm that no correction is applied in this case.

In order to assess the particle rate from the source, data have been collected with the internal trigger, by opening random acquisition windows of 625 ns each.[2] After data cleaning and clusterization, as above described, the number of resulting clusters has been counted (each reconstructed cluster is assumed to belong to an independent ionizing event). The rate has been finally calculated by dividing the total number of reconstructed clusters by the overall acquisition time. The rate as a function of the amplification voltage for different attenuation filters is shown in Fig. 5, and, in a preliminary version, in Ref [9]. At full particle rate, equivalent to attenuation filter 1, a maximum gamma conversion rate of about 120 kHz/cm^2 has been measured. It is important to notice that even at the highest photon rate a plateau in the rate is reached, meaning that the detectors are fully efficient to incoming particles starting from about 520 V. At lower voltages, the amplification is lower, leading to a reduction of the cluster finding efficiency.

The differences of the event topologies resulting from detector exposure to the GIF++ photon spectrum or to muons reflect themselves in the cluster charge distributions as shown in Fig. 6. Muons, with the detector operated at an amplification voltage of 500 V, deposit a charge of about 1200 ADC counts (Most Probable Value, MPV) traversing the 5 mm drift gap, their charge distribution is Landau like. The charge distribution generated by photons looks very different, it has its maximum at very low charges and decreases continuously with a non-negligible tail to charges exceeding those of muons.

5. Simulation

A Geant4 simulation[3] has been implemented in order to predict the response of the detector to the GIF++ photon spectrum and to estimate the current induced by irradiation in the chambers. The GIF++ spectrum is characterized by a wide range of photon energies, spanning from 0 to 662 keV, and dependent on the position in the facility and the attenuation filter setting. The 662 keV peak accounts for about half of the overall photons. In order to achieve a detailed comprehension of the detector response to this complex spectrum, two steps of the simulation have been carried out. The first consisted in the characterization of the detector, when illuminated by monochromatic photons impinging perpendicular on the detector. Photon energies have been simulated, from 10 to 662 keV. The second step consisted in the simulation of the GIF++ source, implemented as a point-like source emitting isotropically photons at 662 keV, of the entire GIF++ facility geometry, as taken from Ref. [11], and of the detector, positioned at its actual position in the facility.

The detector geometry has been implemented starting from an already validated and very detailed modelling of a Micromegas chamber [12]. The drift and the amplification gaps have been defined as active volumes in the simulation.

5.1. Detector response in a mono-energetic photon beam

Energy deposited in the gas leading to the formation of a signal may be due to two types of events. On one side, photons interacting via Compton or photoelectric effect in the gas lose part of their energy by ionization in the gas. The second case concerns events in which the

[2] Data can be acquired according to two different methods: either the trigger signal is generated externally, as for example, by scintillators, or internally, from an internal clock. The latter is used for taking the pedestal level, the external trigger is used for the data taking during beam time.

[3] The physics models used in the two simulations have been chosen to be QGSP BIC [10].

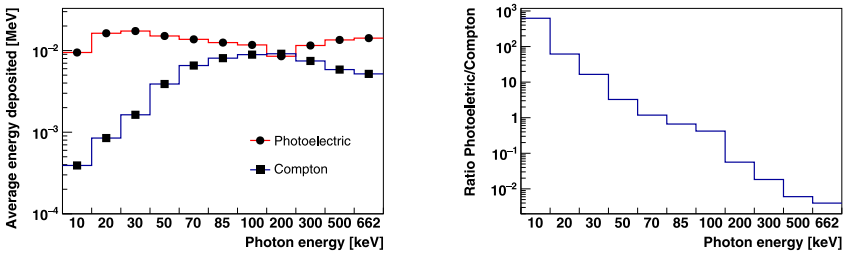

(a) (b)

Fig. 9. Average energy deposited in events where photoelectric (red) and Compton (blue) processes take place in the gas (a). Ratio between number of events where photoelectric effect took place and those with Compton scattering.

photon interacts somewhere else in the detector structure (as in the metallic mesh, for example) and some of the secondary electrons reach the sensitive region. The relative probability of the two event types to take place depends on the photon energy and is shown in Fig. 7. The vast majority of the interactions happens in the detector material and only a small fraction in the gas. It can be seen that the probability for a signal to be caused by a photon interaction in the gas decreases, in general, as the photon energy increases.

The two event typologies are rather different from the point of view of the amount of energy deposited in the gas, as shown in Fig. 8. The red line shows the average energy deposited by all events, without any condition on the place of a photon interaction, while the blue one concerns only events where the primary photon interacted in the gas. The interaction of a photon in the gas is shown to lead to a higher energy deposition in the gas than for those events where the photon interacts in the material. In the range below 50 keV the deposited energy is remarkably higher than at higher photon energies.

For the interactions in the material, whatever the primary energy of the photon, the average energy deposited in the gas does not change much, reaching a value between 3 and 4 keV per event.

For the interactions in the gas, the individual contributions from Compton scattering and photoelectric effect are shown in Fig. 9(a). Events where the photon interacts via the photoelectric effect deposit on average more energy than the ones where the photon interacts only via Compton scattering, especially at lower energy. Fig. 9(b) shows the ratio between the number of interactions via photoelectric effect and those where Compton scattering took place as a function of the energy of the photon. As seen in Fig. 9(b), at lower photon energy the probability of undergoing a photoelectric effect interaction is dominant, above 70–80 keV energy Compton scattering takes over.

5.2. Detector response in the GIF++ facility

The second step of the simulation was to reproduce as accurately as possible the experimental setup at GIF++. The GIF++ facility geometry has been imported in the Geant4 project as *GDML* file, as used in Ref. [11]. The detector has been placed at 90 cm from the source, i.e. at the same position used during the experimental campaign. The source is modelled as an isotropic source of photons at an energy of 662 keV; the full system of lenses, and lead shields is modelled as well, allowing us to reproduce the spectrum according to different source attenuation filters.

The main goal of the simulation was to estimate how the choice of attenuation filters influences the current observed in the detector. As in the simulations without the GIF++ setup, two types of events can be distinguished: events where the photons interact in the gas, and events where the photons interact in the detector material and only secondary electrons travel into the gas. As shown in Fig. 10, in most of these events the primary photon interacts in the detector structure, in particular the external Mylar window, the drift structure, the metallic mesh, the aluminium frame and the detector PCB, but also in the facility

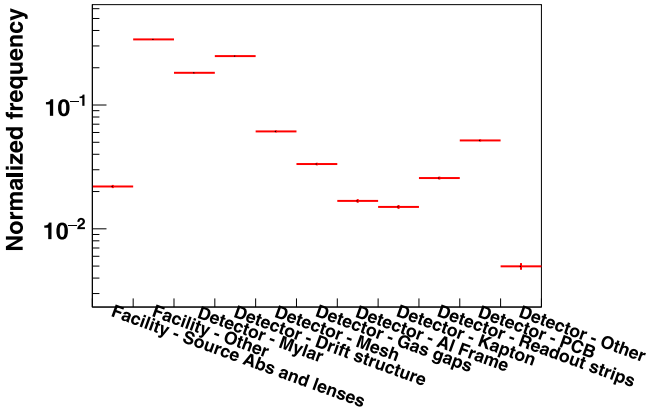

Fig. 10. Location in the facility of primary photon interaction in events leading to a signal in the detector.

structure, such as the source absorber and lenses. Only 2%–3% of the interactions happen in the gas.[4] The energy distribution of the primary photons is shown in Fig. 11(a), while the energy distribution of only those ones interacting in the gas is reported in Fig. 11(b): the majority of interacting photons have an energy above 500 keV, in agreement with the source spectrum. The relatively large contribution from low energy photons is explained by the higher interaction cross-sections.

Fig. 12 shows the energy deposited in the gas per event, for all event types (a) and as a function of different attenuation filters (b). The mean value of about 4 keV is independent of the filter setting and in agreement with what was observed in the simulations without the GIF++ setup.

6. Results

6.1. Performance under high particle rate

One of the goals of this work is to evaluate the detector behaviour in a high photon background environment. For this purpose the detector response to high energetic muons has been studied in the presence of gamma background, combining the GIF++ gamma field with the CERN SPS muon beam.

The two Micromegas detectors under study (T5 and T8) have been installed in a telescope aligned to the muon beam as shown in Fig. 13. Two other 10 × 10 cm^2 Micromegas detectors (Tmm5 and Tmm6) have been used as tracking chambers. The trigger signal was generated by the coincidence of scintillators placed both outside and inside the facility. Fig. 14 shows the charge deposited by a muon track in all

[4] This value covers the full gas volume of the detector; the interactions in the drift and amplification gaps account only for roughly 1/3 of this figure.

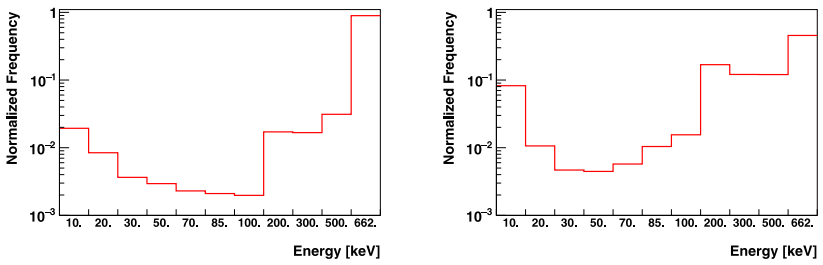

Fig. 11. Energy distribution of photons interacting in the detector and in the facility leading to a detectable signal in the gas (a). Energy distribution of photons interacting in the gas (b).

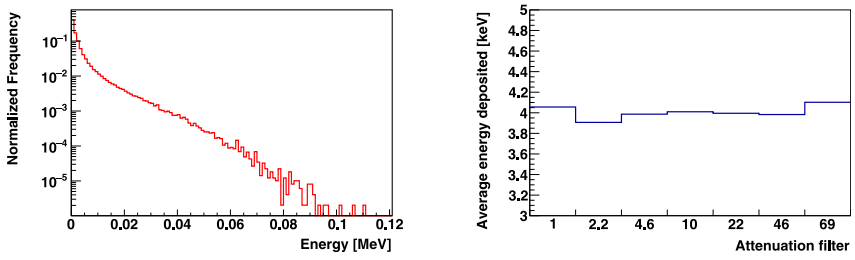

Fig. 12. Energy deposited in the gas per event (a). Average energy deposited per event as a function of the attenuation filter simulated (b).

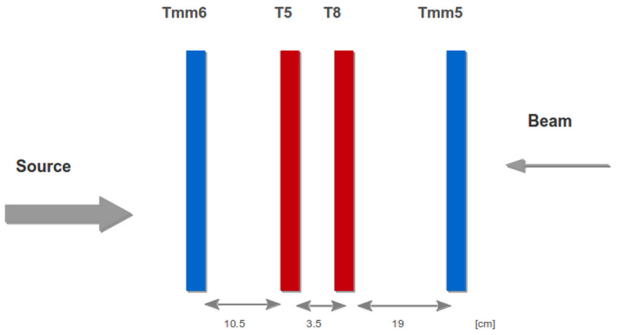

Fig. 13. Setup for the high-rate detector performance study. Two bulk Micromegas (Tmm5 and Tmm6) are used as tracking chambers, T5 and T8 are the chambers under study.

four detectors in the presence of low photon background from the source. Tmm5 and Tmm6 chambers (in the following indicated as Tmm chambers) have two readout layers with 250 μ m strip pitch in X and Y. T5 and T8 chambers (in the following indicated as *T* chambers) were placed back-to-back. This is the reason that the T5 and T8 signals do not appear at the same strip number. In this event display there is a muon track and a photon hit. In T8, there are two clusters, one produced by the muon track peaked around strip number 76 and one is from a background photon with the cluster just below strip number 50. As seen in the right panels, the background hit arrives, in this example, about 150 ns after the track signals.

To distinguish between photon and muon tracks, the Hough transform method has been adopted [13]. The technique is based on a phase-space transformation from the spatial to the Hough space by means of linear (or more complex) equations. After the topological reconstruction of the events, each cluster is translated into a line, or a curve, in the Hough space, by taking into account the position of each detector in the beam-line; clusters compatible with originating from the same ionizing particle intersect in a point in the Hough space, whose coordinates, when anti-transformed, provide for the track parameters.

The particle background rate has been varied by changing the source filter from 0 up to about 70 kHz/cm^2. The rate estimation is described in the following section. The detector amplification as a function of the particle rate, has been inferred from the cluster charge of muon candidates.

Fig. 15(a) shows the Most-Probable-Value (MVP), obtained from the fit of the muon cluster charge distribution with a Landau function, as a function of the background rate, measured with the detector operated at an amplification voltage of 500 V. Only for the data point at 70 kHz/cm^2 a small reduction is observed. The resolution of the detectors has been obtained comparing the measured cluster position in T5 and T8 with the one expected from the track obtained from the Tmm detectors; the residual distribution is then fitted with a Gaussian distribution whose sigma parameter represents the resolution. Fig. 15(b) shows the resolution as a function of the background rate. The spatial resolution obtained from the fit of the residuals is ~70 μ m, including the track fit uncertainties, up to 70 kHz/cm^2. A preliminary version of the same results can also be found in Ref. [14]

These results confirm the good performance of these detectors when operated in a high particle-rate environment, making them a very attractive solution for new experiments or experiment upgrades at the LHC.

6.2. Sensitivity estimation

The detector sensitivity is defined as the probability that a photon passing through the active detector region is detected. The photon rate impinging on the detector for different attenuation filters has been estimated in the Geant4 simulations. The gamma conversion rate has been obtained from the measurement shown in Fig. 5 considering the detector in full efficiency above 520 V amplification voltage, as will be shown in Section 6.4. The sensitivity is calculated as the ratio between the two values and is reported in Table 1 for a few different values of the source filters. A sensitivity of about 0.0025 is obtained, except

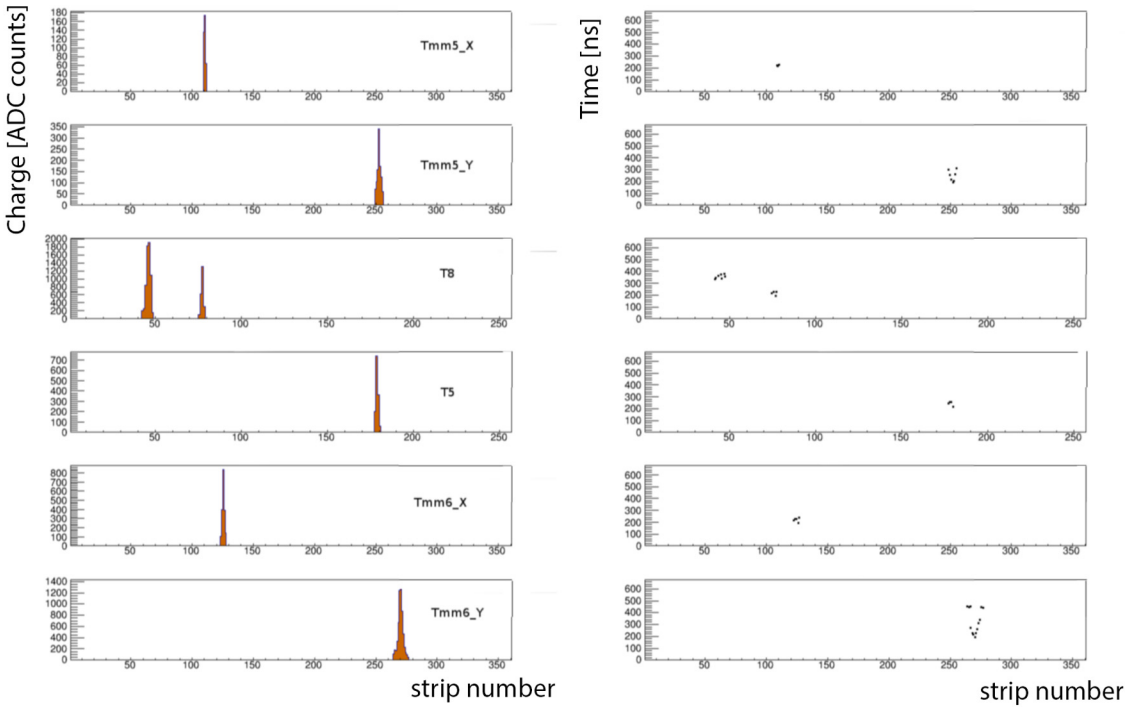

Fig. 14. Event as shown in the Online software of a muon crossing the T/Tmm telescope plus an additional background photon interaction in T8. The left panel shows the charge deposited in the Tmm (x and y positions) and T detectors as a function of the strip number, while the right panel shows the time at which the charge is scored.

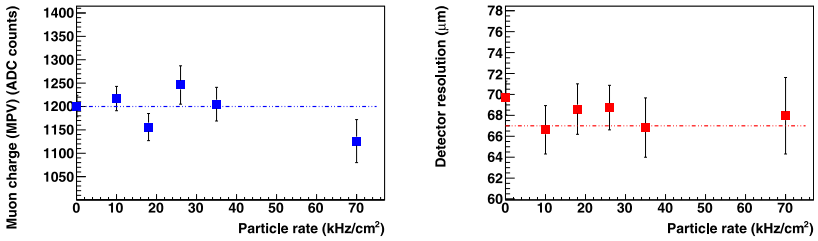

Fig. 15. Most-probable-value of the muon charge (a) and resolution (b) as a function of the particle rate. The error bars refer to the error obtained from the fit.

Table 1
Gamma conversion rate and sensitivity as obtained for different attenuation filters.

Att filter	Geant4 gamma Rate (kHz/cm^2)	Measured gamma conversion Rate (kHz/cm^2)	Sensitivity
1	$5.7 \cdot 10^4$	115	0.0020
1.5	$3.9 \cdot 10^4$	99.13	0.0026
2.2	$2.7 \cdot 10^4$	68.05	0.0025
4.6	$1.3 \cdot 10^4$	34.59	0.0025
10	$7.0 \cdot 10^3$	18.16	0.0026
100	$1.05 \cdot 10^3$	2.54	0.0024

when the source is not shielded (Att=1). In this case, a lower value has been found; this effect is most probably due to an underestimation of the measured gamma conversion rate caused by a saturation of the clustering algorithm.

6.3. Current

Fig. 16 shows the current on the resistive strips (in log scale) as measured by the power supply as a function of the amplification voltage

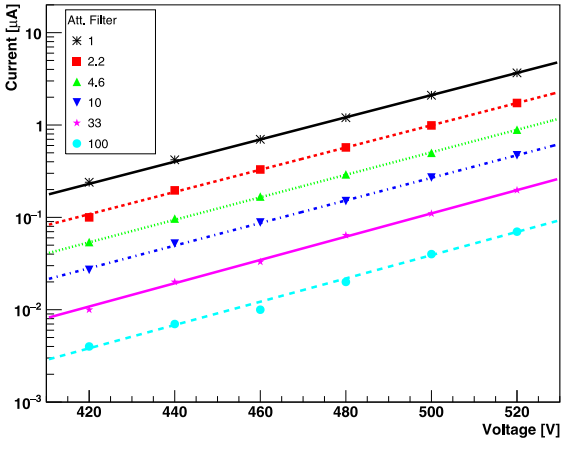

Fig. 16. Detector current in log scale as a function of the amplification voltage for different attenuation filters. The markers represent the measured data and the lines correspond to the exponential fits in log scale.

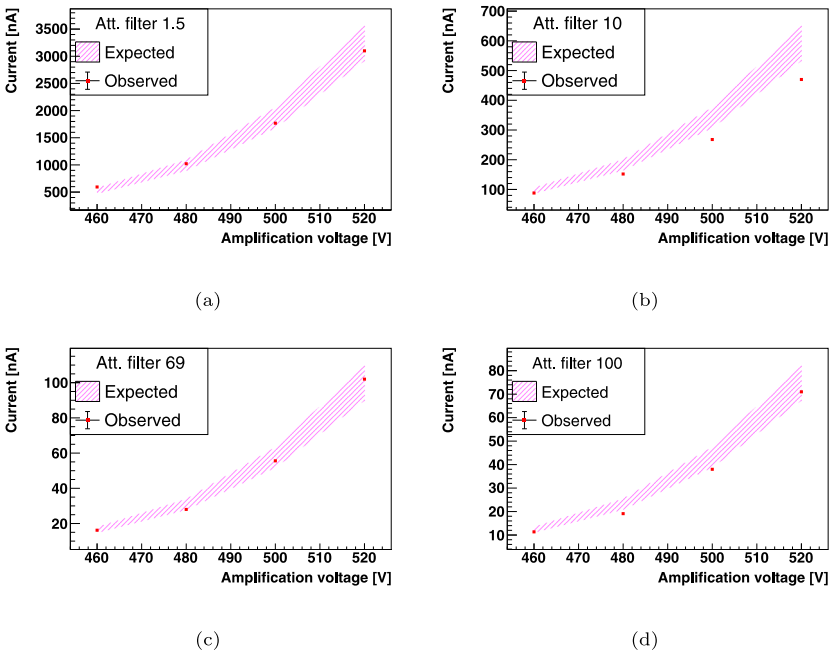

Fig. 17. Estimated current compared with measured values for different attenuation filters as a function of the amplification voltage.

for different values of the attenuation filter from 1 (no attenuation) to 100 (factor 100). As expected, increasing the amplification voltage results in an increase of the current due to an increase of the gain. Lower attenuation results in an increase of the hit rate on the detector, consequently leading to an increase of the current.

The current has also been estimated from the measured rate according to the following formula:

$$I = rate_{max} \cdot Area \cdot E_{dep}/26\ (\text{eV}) \cdot e \cdot G \tag{1}$$

where $rate_{\max}$ is the gamma conversion rate as shown in Table 1, *Area* is the active region area, equal to 100 cm^2, E_{dep} is the average energy deposited per event as obtained from the simulation in Fig. 12, 26 eV is the argon ionization energy, e is the electron charge and G is the detector gain as measured in the laboratory, see Fig. 20 in Section 6.4. Figs. 17 shows the expected current compared to the measured one as a function of the amplification voltage for four values of the attenuation filter (1.5, 10, 69, and 100). A 10% error on the estimated values has been considered, taking into account uncertainties on the gain measurement, particle rate estimation and average energy deposited. A good agreement is observed.

6.4. Long-term ageing studies

Long-term exposition to ionizing radiation may induce a degradation of the detector performance. Assessing and quantifying such effects is of utmost importance in the characterization of detectors to be installed in experiments such as ATLAS and CMS and supposed to work for a long time without possibility for replacement. In this study two Micromegas detectors, T5 and T8, have been exposed to the GIF++ background to perform accelerated ageing. The two detectors were operated with an Ar:CO_2 gas mixture (93:7), at a reference amplification voltage of 500 V. The data discussed here were acquired between June 2015 and December 2017. The initial goal was to accumulate the charge expected in 10 years of HL-LHC operations, considering the particle rate expected in the inner forward muon station regions. This integrated charge has been estimated to be about 0.2 C/cm^2. The test finished in December 2017, after accumulating more than 0.3 C/cm^2, exceeding the initial goal. Throughout the long-term irradiation period, the detector current, HV settings, environmental conditions in the bunker have been constantly monitored. The accumulated charge

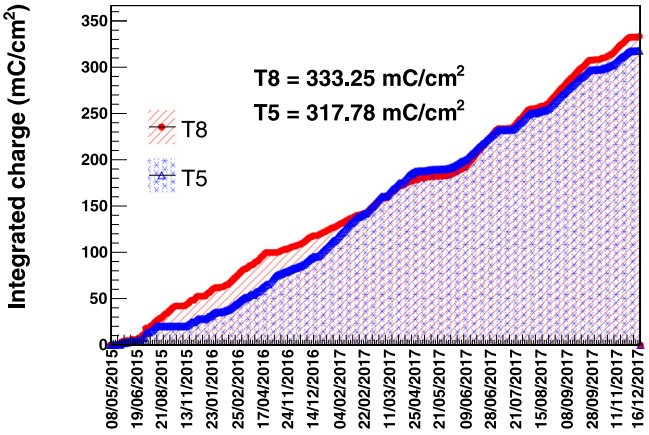

Fig. 18. Integrated charge as a function of time.

calculated integrating the instantaneous current in the detectors is shown in Fig. 18. It is evident that the charge accumulation rate, i.e. the slope of the two curves, is not constant throughout the time. This is due to the frequent changes in the detector position, which affect the particle rates impinging on the detectors, and changes in the source attenuation settings.

The detector gain and the efficiency to muons have been measured before the start of the irradiation, after accumulating an integrated charge of about 0.1 C/cm^2 in 2016, and finally at the end of the irradiation period with a total integrated charge of about 0.3 C/cm^2. Fig. 19 shows the detector efficiency to muons as a function of the amplification voltage for both detectors, T5 and T8, for the three data taking campaigns. Data have been taken profiting of the CERN SPS muon beam available in the GIF++ facility and using 2D Micromegas detectors as tracking chambers. During these measurements the source had been completely shielded to avoid photon contamination. The detector is considered efficient if exactly one cluster is found on each tracking chamber and if the cluster is reconstructed within 500 μ m from the expected position on the detector under test. If no clusters are found or the cluster is reconstructed outside the 500 μ m window, the detector is considered inefficient.

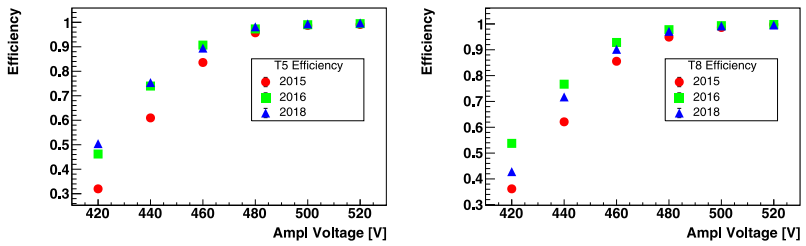

(a) (b)

Fig. 19. Detector efficiency as a function of the amplification voltage for T5 (a) and T8 (b) for the three data taking campaigns: 2015 in red, 2016 in green and 2018 in blue.

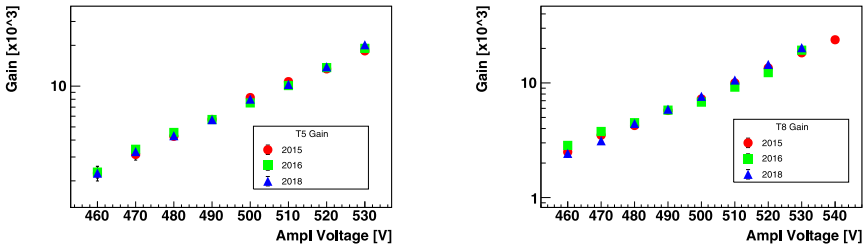

(a) (b)

Fig. 20. Gas gain for T5 (a) and T8 (b) as a function of the amplification voltage for the three measurements: 2015 in red, 2016 in green and 2018 in blue.

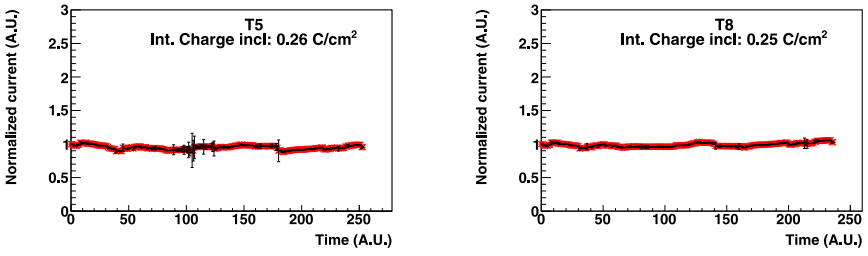

(a) (b)

Fig. 21. Current trend for T5 (a) and T8 (b) as a function of time.

Two main aspects should be considered in the evaluation of the efficiency. The first and most relevant is the efficiency reached at the plateau; a degradation of this value implies a unavoidable loss of tracking capabilities. The second one is the working point, namely the voltage at which the detector reaches the maximum efficiency. An increase of the working point, possibly due to a local partial shielding effect of the electric field, would require the detector to be operated at higher voltages, leading to instabilities and discharges. As clearly shown in the plots, none of the two effects took place in the detectors. At lower voltages, which means lower amplification, a discrepancy among the data taking campaigns is found, explained by different environmental conditions, whose effect is not taken into account in the present study.

The gas gain measurements have been performed in the laboratory with a ^{55}Fe source after removing the chambers from the GIF++ facility. For this measurement, the mesh is connected to a discriminator and to a scaler to measure the rate of photons imping onto the detector once the source is placed on top of the chambers. The gas gain is then calculated measuring the current on the resistive strips according to the following relation:

$$G = \frac{I}{R \cdot e \cdot p}, \tag{2}$$

where R is the photon rate measured on the mesh, e is the electron charge, and p is the average number of ionization electrons expected to be produced once a photon interacts in the gas, in our case p≃200. Fig. 20 shows the gas gain for both chambers as a function of the amplification voltage for the three measurement campaigns in 2015, 2016 and 2018. Corrections for different environmental conditions are not applied. No reduction of the amplification is observed.

An additional method to assess the detector ageing was to monitor the detector current throughout the 2.5 years of irradiation. This method suffers from the frequent changes of the source attenuation settings and from movements of the detectors. In order to account for this issue an *ad hoc* method has been developed. First, time intervals where detector and source conditions are unchanged are found: if, for example, at a certain instant, the attenuation filter is moved, then that specific time interval is closed and a new one is started. These intervals, in general few days long, represent our basic time unit. Subsequently these time intervals are joined together: the current is rescaled in such

a way that the very first part of a period takes the same value of the last part of the previous one. With this method, despite losing the absolute value of the current, we are still able to detect a trend in the current, if any. Another aspect that has to be taken into account is the charge-up and polarization of the dielectric material as soon as the source is opened at very high-rate. When the source is opened, a very high current is recorded, but followed by a sudden, few seconds, drop of about 20%. This reduction is then followed by a later and much slower increase, which could last several minutes, of a few percent. The current is stable thereafter. In order not to bias the analysis with these transient effects, the very first part of each time unit is removed in order to include only stable conditions. Fig. 21 shows the current behaviour for the two chambers as a function of the time units. The integrated charge considered in the analysis is slightly lower than the total accumulated one due to the constraints previously described, in particular the data cleaning needed in order to avoid biases due to transient detector effects. In any case, both detectors do not show any trend in the current behaviour and no appreciable changes are observed, as already suggested by the two previous methods.

7. Conclusions

An extensive study of the performance of two 10×10 cm^2 resistive Micromegas, operated with an Ar:CO_2 gas mixture (93:7), has been performed at the CERN GIF++ facility. The aim was to assess a possible degradation of the detector performance either at high background rates or/and after a long-term exposure to ionizing radiation equivalent to the life-time of HL-LHC experiments. The detectors showed no performance degradation up to background rates of 70 kHz/cm^2, much in excess of the 10 kHz/cm^2 expected at HL-LHC in the inner forward muon station of ATLAS. After 2.5 years of irradiation with an accumulated charge of more than 0.3 C/cm^2, corresponding to 15 years of HL-LHC operation, no degradation of the detector performance was observed.

In addition, a Geant4 simulation campaign has been carried out to better understand the detector response to the GIF++ photon background. It showed that the overwhelming majority ($\geq$ 98%) of the photon interactions that lead to a signal happen in the detector material and not in the gas gaps themselves. For the GIF++ photon spectrum the average probability that a photon interacts in the detector and is detected was found to be 0.0025. The energy that is deposited in the gas gaps has a strongly falling spectrum, with an average of 4 keV, almost independent of the initial photon energy.

Declaration of competing interest

The authors declare that they have no known competing financial interests or personal relationships that could have appeared to influence the work reported in this paper.

Data availability

Data will be made available on request.

Acknowledgements

The studies presented here benefited from the contributions of several groups. In particular we wish to thank the GDD laboratory at CERN and the CERN Micro-Pattern Technologies workshop for their continuous and fruitful collaboration in the detectors development and characterization and the GIF++ team for the successful operation of the facility. Special thanks go to D. Pfeiffer for providing us with the GIF++ model geometry used in these studies and to N. Karastathis, for implementing and validating the Geant4 template of the Micromegas detectors used in our simulations.

References

[1] S. Zimmermann High-Rate and Ageing Studies for the Drift Tubes of the ATLAS Muon Spectrometer, CERN-THESIS-2004-018.
[2] M.R. Jaekel, et al., CERN GIF++, PoS (TIPP2014) 102.
[3] Y. Giomataris, Nucl. Instrum. Methods A 419 (1998) 239.
[4] T. Alexopoulos, et al., Nucl. Instrum. Methods A 640 (2011) 110.
[5] ATLAS Collaboration, ATLAS New Small Wheel Technical Design Report, ATLAS-TDR-10, CERN-LHCC-97-022.
[6] Geant4 Collaboration, Geant4–A simulation toolkit, Nucl. Instrum. Methods A 506 (2003) 250–303, http://dx.doi.org/10.1016/S0168-9002(03)01368-8.
[7] M. Raymond, et al., IEEE Nucl. Sci. Symp. Conf. Rec., vol. 2, 2000.
[8] S. Martoiu, et al., J. Instrum. 8 (2013) C03015.
[9] B. Alvarez Gonzalez, et al., Performance studies under high irradiation of resistive bulk-Micromegas chambers at the CERN Gamma Irradiation Facility, PoS (ICHEP2016) 1216.
[10] Geant4 Reference Physics Lists. https://geant4.web.cern.ch/node/302.
[11] D. Pfeiffer, et al., Nucl. Instrum. Methods A 866 (2017) 91–103.
[12] N. Karastathis, RD51-NOTE-2015-011.
[13] R. Fisher, S. Perkins, A. Walker, E. Wolfart, Hough transform, 2003, URL: http://homepages.inf.ed.ac.uk/rbf/HIPR2/hough.htm.
[14] E. Farina, et al., Ageing and high rate studies on resistive Micromegas at the CERN Gamma Irradiation Facility, PoS (ICHEP2018) 665.